

Nuclear reaction measurements of 80.5 MeV/u ^{12}C beam bombarding on C, W, Cu, Au, Pb targets

Zhichao Gao^{a,b}, Xueying Zhang^{a,b}, Yongqin Ju^a, Liang Chen^a, Honglin Ge^{a,*},
Yanbin Zhang^a, Fei Ma^a, Hongbin Zhang^a, Guozhu Shi^a, Zhiqiang Chen^{a,b},
Rui Han^{a,b}, Guoyu Tian^a, Fudong Shi^a, Bingyan Liu^{a,b}, Xin Zhang^{a,b}

^a*Institute of Modern Physics, Chinese Academy of Science, Lanzhou 730000, China*

^b*School of Nuclear Science and Technology, University of Chinese Academy of Sciences,
Beijing 100049, China*

Abstract

To get the energy spectrum distribution and cross-sections of emitted light charged particles and explore the nuclear reaction, a experiment of 80.5 MeV/u ^{12}C beam bombarding on C, W, Cu, Au, Pb targets has been carried out at Institute of Modern Physics, Chinese Academy of Science. 30° , 60° and 120° relative to the incident beam have been detected using three sets of telescope detectors. The method of ΔE - ΔE - E was used for particle identification. The results indicate that there is a tendency that heavier targets have larger double differential cross-sections and the emitted fragments are more likely to go forward. Besides, the decrease of cross-sections of fragments producing with the increasing emitted angles may follow some kind of pattern.

Keywords: nuclear reaction, heavy target, energy spectrum, cross-section

1. Introduction

Heavy ion nuclear reactions refers to the nuclear reactions caused by ions heavier than α particles. With the development and improvement of heavy ion accelerator technology, recently, people have been able to accelerate almost
5 all the stable nuclides existing in the nature to the energy sufficient to cause

*Corresponding author

Email address: hlge@impcas.ac.cn (Honglin Ge)

nuclear reaction. The possible reaction systems have been greatly expanded, and abundant experimental phenomena not found in light ion nuclear reactions have been observed. Nowadays heavy ion nuclear reaction has become the main field of nuclear physics research . The heavy ion nuclear reaction offers an opportunity
10 to study phase transition in nuclear matter [1], the nuclear equation of state [2] and the properties of high temperature and high density nuclear matter [3]. As carbon is an important component of cosmic rays [4], experiments of carbon beams bombarding on targets are also used to study the radiation risks of people on space missions.

15 For the purpose of improving the dose deposition accuracy of hadron therapy, many countries have carried out experiments of carbon beams of different energies bombarding on varieties of targets. Measurements of total and partial cross-sections of fragments for incident ^{12}C beams in water and polycarbonate at energies ranging from 200 to 400 MeV/u were made by Japan scientists (T.
20 TOSHITO et al.) in 2004 [5]. In 2008, to extend these data to lower energy, France scientists performed an experiment of a 95 MeV/u ^{12}C beam on thick PMMA targets [6]. They performed another experiment on thin targets to study C-C, C-H, C-O, C-Al and C- $^{\text{nat}}\text{Ti}$ reactions at 95 MeV/u in 2011 [7]. In the same year, the FIRST collaboration performed an experiment of 400 MeV/u
25 ^{12}C beam on carbon target at GSI [8]. And M De Napoli et al. [9] and T. Ogawa et al. [10] also performed different experiments of ^{12}C fragmentation reactions in order to test the ability of nuclear models to reproduce the fragments production.

Our team has been engaged in experimental research in heavy ion nuclear
30 physics[11, 12, 13, 14], to learn more about the fragmentation reaction of ^{12}C , we have carried out an experiment of 80.5 MeV/u ^{12}C beam bombarding on C, W, Cu, Au and Pb targets. The energy spectrums and cross-sections of light particles have been measured at 30° , 60° and 120° away from beam. The experimental setup will be presented in detail in section 2.

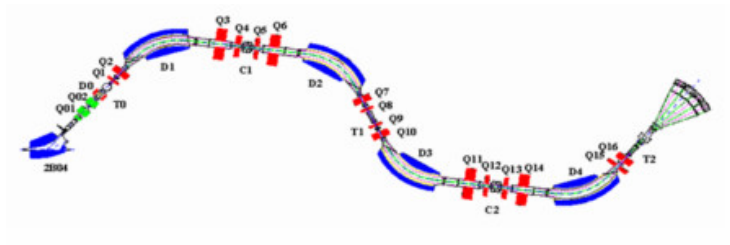


Figure 1: The schematic diagram of RIBLL.

2. Experimental setup

The experiment was performed at The Radioactive Ion Beam Line in Lanzhou (RIBLL) at the Heavy Ion Research Facility of Lanzhou (HIRFL) [15]. Fig. 1 shows the schematic view of RIBLL.

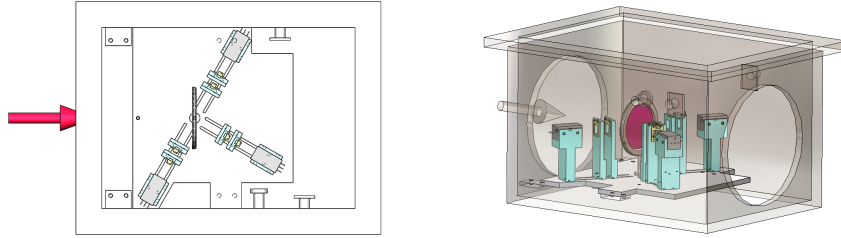
We have measured the double differential cross sections of an 80.5 MeV/u ^{12}C beam bombarding on five different thin targets at three angles: 30° , 60° and 120° . The thickness and area density ($\rho \times \text{length}$) of Pb, W, Cu, Au, C targets are listed in Table 1.

The experiment was carried out in T2 target chamber. The layout of this experiment is shown in Fig. 2. There is a plastic scintillator detector as beam monitor placed before the target chamber. It monitors the beam state by recording the number of particles. The beam intensity of ^{12}C beam during the experiment was about 10^6 ions/s.

Table 1: Parameters of targets.

Target	Pb	W	Cu	Au	C
Thickness (mm)	0.15	0.15	0.05	0.1	1
Area density (mg/cm^2)	170.2	290.3	44.8	193.2	185

The beam hit on the center of the target, which was fixed on the chamber. Since the targets were very thin, most of the fragments could penetrate them. These fragments were detected by three sets of same ΔE - ΔE - E telescope detectors, which were fixed at 30° , 60° and 120° with respect to the beam line,



(a) The target chamber from the top view. (b) The three dimensional schematic diagram of the target chamber.

Figure 2: The schematic diagram of experiment layout.

as shown in Fig. 2. The parameters of these telescope detectors are listed in Table 2. Each set of the telescope detector consists of two Si detectors and one scintillator detector. The two Si detectors are $300 \mu\text{m}$ and $1000 \mu\text{m}$, followed by a CsI detector with a thickness of 5 cm. The distance between the center of the target and the first Si detector is 10 cm. 55

Table 2: Parameters of one set of telescope detectors.

	Detector 1	Detector 2	Detector 3
Type	Si	Si	CsI
Thickness	$300 \mu\text{m}$	$1000 \mu\text{m}$	5 cm
Distance from the target	10 cm	11.5 cm	13 cm
Size	25.4 mm \times 25.4 mm		
Ω	48.9 msr		

The particles are measured when they have just enough energy to pass through the first Silicon detector and reach the second stage of detector. So the distance between the target and the second Stage of the detector, which is 60 11.5 cm, is used to calculate the acceptance of the telescope detectors. Since the size of the detectors is $25.4 \text{ mm} \times 25.4 \text{ mm}$, the acceptance Ω is calculated to be 48.9 msr.

3. Data processing

3.1. Particle identification

65 Particles with the same incident energy and different mass and charge lose
different energies in the same material. Therefore, the particles can be identified
by the telescope detectors because the deposited energy is related to their mass
and charge. Fig. 3 represents the particle identification map between the first
silicon detector and the second silicon detector and the map between the second
70 silicon detector and the CsI detector. It is clear that there are several separate
belts in the maps. It is explicit to distinguish the particles - p, d, t, ^3He and
 ^4He , as shown in Fig. 3. The left-hand figure shows the particles punch through
the first stage of the telescope, which is a silicon detector of $300\ \mu\text{m}$. And the
right-hand side figure only presents the particles which have enough energy to
75 punch through $1300\ \mu\text{m}$ silicon.

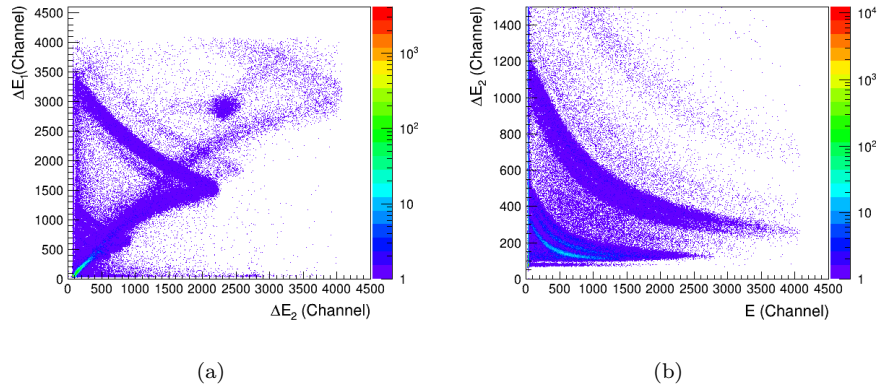


Figure 3: The first picture is the particle identification map between the first stage and the second stage of the telescope. The second picture is the particle identification map between the second stage and the third stage of the telescope. Both of them are the identification map of target-Pb at 30° .

3.2. Energy calibration

Energy calibration is the most important step in data processing, which is related to the double differential cross-section of the particles. Fig. 3(a) is used

to calibrate silicon detectors. Since the horizontal axis and the vertical axis are
 80 the channel of the second and the first stage of the axis, the back bending of
 each belt corresponds exactly to the particles which have just enough energy to
 punch through the second stage of the telescope detector. The rate of energy
 loss of each particle and each energy is available through the SRIM software [16].
 With the corresponding of the punch through energies obtained by SRIM and
 85 the punch through channels obtained by the identification map, the calibration
 curves of the silicon detectors are obtained. One silicon detector is calibrated
 only once, because its linear relationship is independent of the charge and mass
 of the particles. As shown in Fig. 4(a), the calibration curve of 1000 μm -thick
 silicon detector is determined by five particles: p, d, t, ^3He and ^4He .

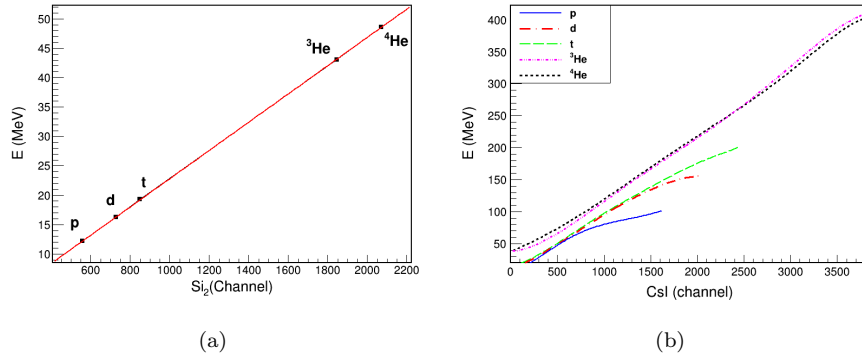


Figure 4: The calibration of the (a) second and the (b) third stage of the telescope.

90 The calibration of CsI detectors is much more complex compared with sil-
 icon detectors. Since the ratio at which a scintillator converts the absorbed
 radiation energy into photons varies for different particles, each fragment needs
 to calibrate for CsI once, as shown in Fig. 4(b). First, considering the linear
 relationship between the channel and the energy of the thick silicon detector,
 95 the vertical axis of Fig. 3(b) can be replaced as the energy of the thick silicon
 detector. Therefore, we can get the relationship between the channel of the CsI
 detector and energy deposited in the thick silicon detector. Second, thanks to
 the SRIM software, it is possible to get the energy deposited in the CsI detector

knowing the energy deposite in the thick sillicon detector. Finally, correspond-
100 ing to step one and step two, we can get the correspondence between the channel
and the energy of the CsI detector.

4. Experimental results

4.1. Energy spectrum at 30°

After the particle identification and energy calibration, it is easy to achieve
105 the double differential cross-sections of each fragment varies with energy at
differents angles.

Fig. 5 shows the energy spectrums for different particles emitted at 30° for
five different targets. The five lines in each figure correspond to five kinds of
fragments emitted at 30° . Compare the figures of different targets, it is clear
110 that the same type of fragment has similar shapes of energy spectrum, regardless
of targets. Besides, for isotopes of $Z = 1$, the double differential cross-sections
decrease as A increases. If we pay attention to the details, the double differential
cross-sections of protons basically remain unchanged until 80 MeV/u , which is
close to our incident energy. And the energy spectrums of deuterons keep flat
115 before 45 MeV and then go down. It is also worth noting that the energy
spectrums of ^3He and ^4He have an intersection at about 60 MeV/u .

For a more intuitive observation, each picture in Fig. 6 combines the enrgy
spectrum of the same fragments at different targets at 30° . It is obvious that the
same fragments have similar energy spectrum distribution for different targets,
120 as proved in Fig. 5. In addition, take Fig. 6(a) as an example, the double
differential cross-section of protons for C target at 30° is smaller than other
heavier targets for less than an order of mangnitude. And that for Cu target
is also a little bit smaller than W, Pb and Au, which may lead to a conclusion
that heavier targets have larger double differential cross-sections of fragments.
125 However, the energy spectrums for W, Pb and Au targets are indistinguishable,
which makes this conclusion more like a tendency. In Fig. 6, we can also observe
that the energy spectrums of protons and deuterons have a flat area at low

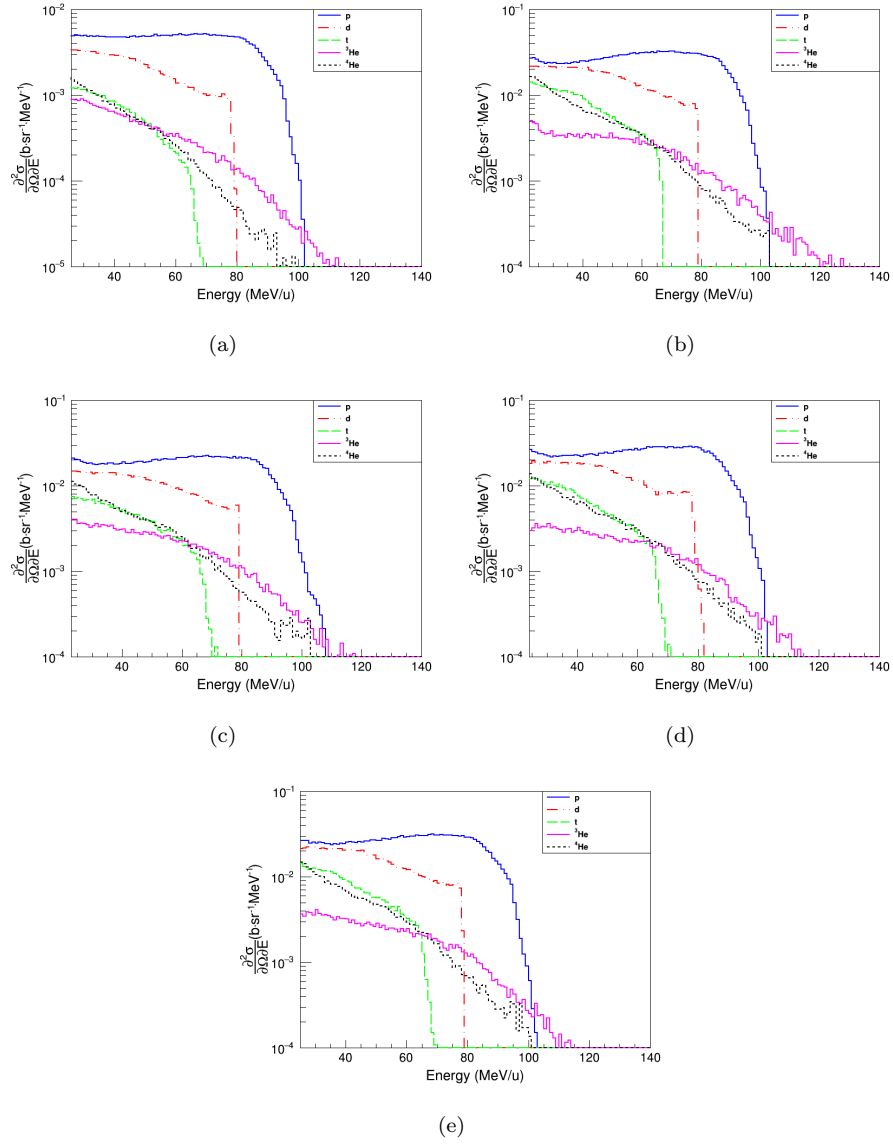


Figure 5: Energy spectrums for different particles emitted at 30° for (a) target-C, (b) target-W, (c) target-Cu, (d) target-Au and (e) target-Pb.

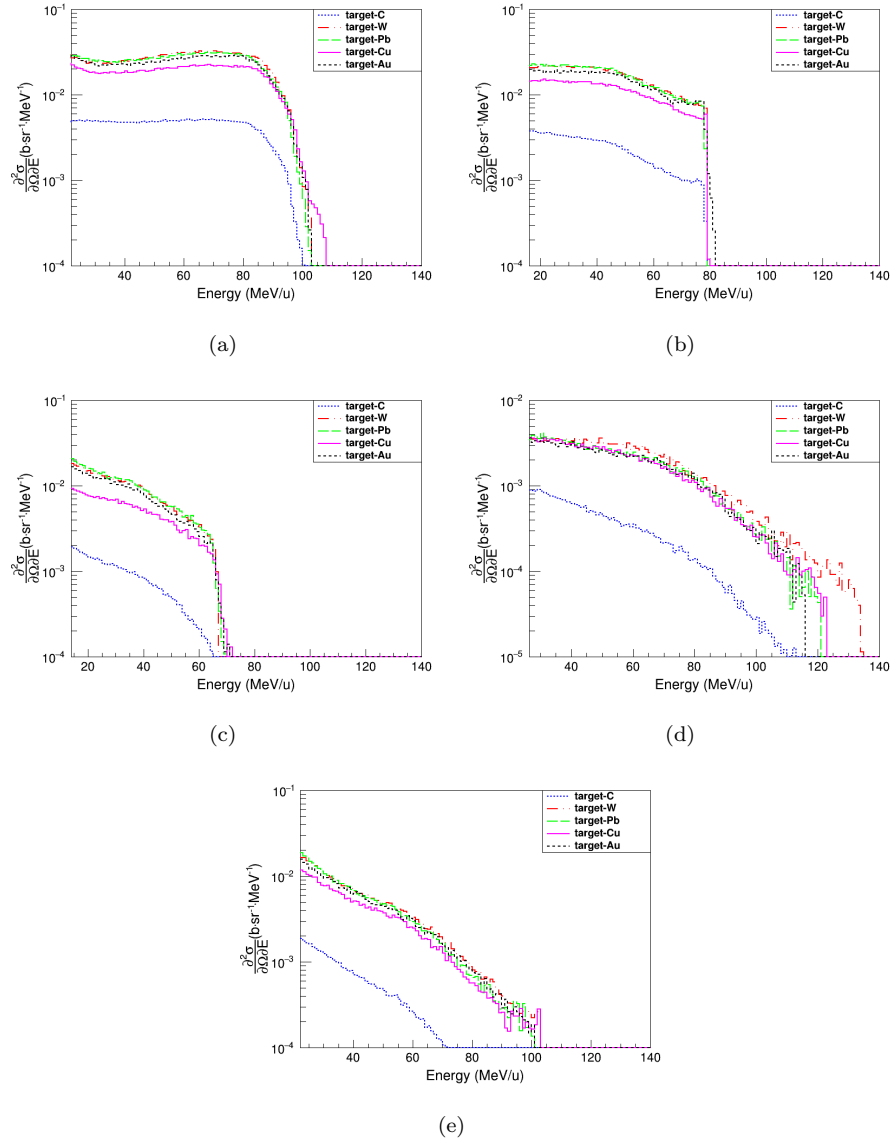


Figure 6: Energy spectrums for (a) p, (b) d, (c) t, (d) ^3He and (e) ^4He emitted at 30° for different targets.

energies and then decrease. However, this phenomenon has not been seen in other fragments.

130 4.2. Energy spectrum at different angles

To describe the spatial distribution of the fragments, Fig. 7 exhibits the energy spectrums for different particles emitted at 30° , 60° and 120° for tungsten target¹. It is obvious that as the emitted angle become larger, the fragments of high energy are much less and the energy spectrum looks more like a straight
135 line when the vertical axis is logarithmic. For isotopes of $Z = 2$, the emitted fragments at 120° are too few to detect. Besides, there is a more significant difference of double differential cross-sections between the three angles for heavier fragments.

4.3. Cross-section

140 The cross-sections have been obtained by integrating the double differential cross-sections of energy. Fig. 8 presents the cross-sections of different particles emitted at 30° , 60° and 120° for tungsten target. This figure can be interpreted in two ways. For a certain emitted angle, the cross-sections of p, d and t decrease exponentially. Second, for a certain kind of fragment, the cross-sections decrease
145 as the emitted angles increase, moreover, this kind of decrease seems to follow some kind of pattern. take ^4He for example, the cross-section difference of 30° and 60° is close to the cross-section difference of ^3He .

5. Summary

150 An experiment of 80.5 MeV/u ^{12}C beam bombarding on C, W, Cu, Au, Pb targets at different angles has been performed at RIBLL. The emitted particles of $Z \leq 2$ were detected at 30° , 60° and 120° relative to the incident beam. The methods of particle identification and energy calibration are introduced in

¹The data of Cu, Au and Pb targets at 60° and 120° was not obtained due to detector malfunction.

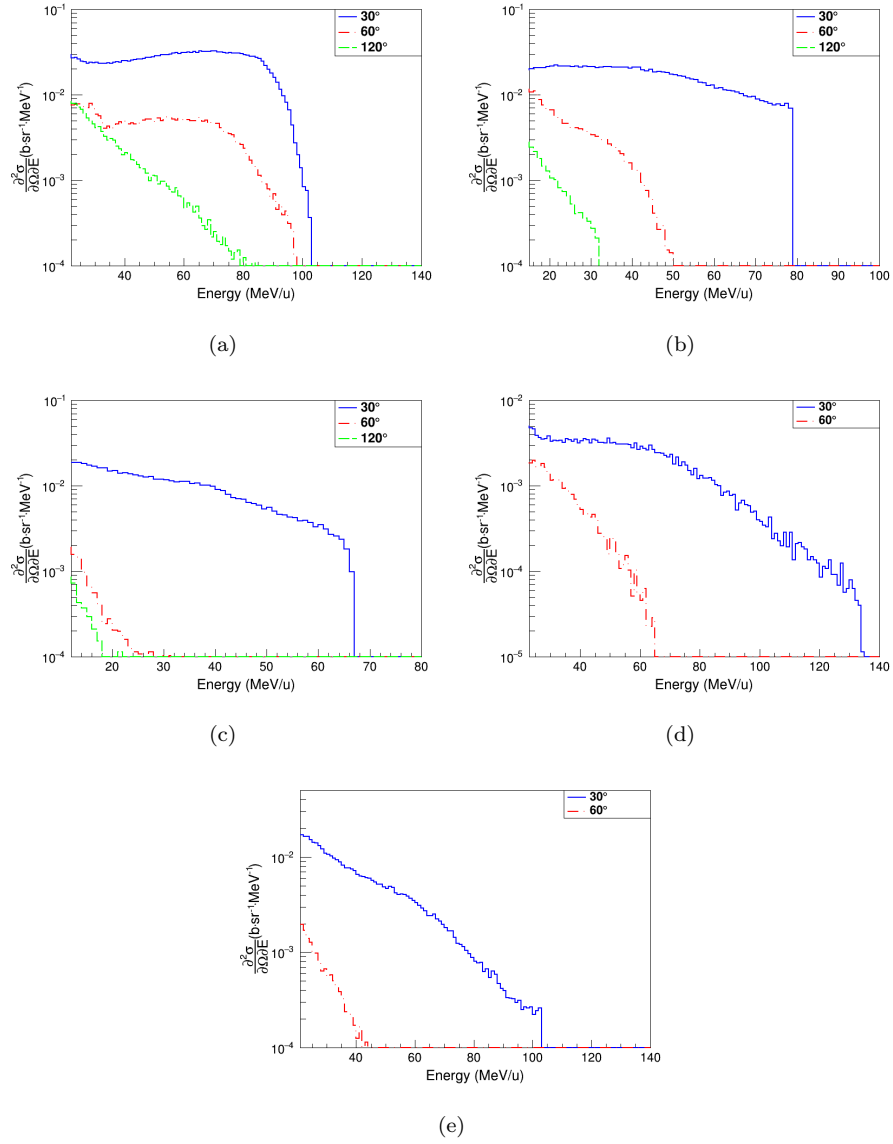


Figure 7: Energy spectrums for (a) p, (b) d, (c) t, (d) ^3He and (e) ^4He emitted at 30° , 60° and 120° for tungsten target.

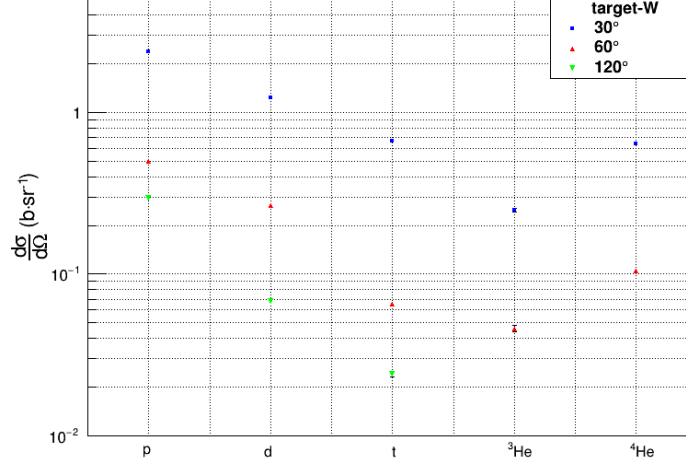


Figure 8: The cross-sections of different particles emitted at 30°, 60° and 120° for tungsten target (only statistical errors are presented).

section 3, and the energy spectrums and cross-sections are presented in section 4. It is apparently that energy spectrums of the same fragments, the same exit angles and different targets have similar shape. The heavy targets have larger double differential cross-sections. At the same time, the double differential cross-sections of target-C are the smallest when all other variables are the same. The cross-sections of the emitted fragments decrease with the increasing emitted angles. Besides, there may be a certain rule in it.

160 6. Acknowledgement

This work was supported by the National Natural Science Foundation of China (No. 11575267, 11775284, 12075296, U1832205, 11875298 and 11605258)

References

- [1] J. Pochodzalla, The search for the liquid-gas phase transition in nuclei,
165 Progress in Particle and Nuclear Physics 39 (1997) 443 – 501. doi:[https://doi.org/10.1016/S0146-6410\(97\)00048-3](https://doi.org/10.1016/S0146-6410(97)00048-3).
- [2] G. Giuliani, H. Zheng, A. Bonasera, The many facets of the (non-relativistic) nuclear equation of state, Progress in Particle and Nuclear
170 Physics 76 (2014) 116 – 164. doi:<https://doi.org/10.1016/j.ppnp.2014.01.003>.
- [3] M. Di Toro, M. Colonna, G. Ferini, T. Gaitanos, V. Greco, H. Wolter, Heavy ion collisions at relativistic energies: Testing a nuclear matter at high baryon and isospin density, Nuclear Physics A 782 (1) (2007) 267 – 274, proceedings of the 5th International Conference on Perspectives in Hadron
175 Physics, Particle–Nucleus and Nucleus–Nucleus Scattering at Relativistic Energies. doi:<https://doi.org/10.1016/j.nuclphysa.2006.10.028>.
- [4] R.A., Mewaldt, The Elemental And Isotopic Composition of Galactic Cosmic Rays (1981) 49 – 68.
- [5] T. Toshito, K. Kodama, L. Sihver, et al., Measurements of total and partial
180 charge-changing cross sections for 200- to 400-MeV/nucleon ^{12}C on water and polycarbonate, Phys. Rev. C 75 (2007) 054606. doi:<https://doi.org/10.1103/PhysRevC.75.054606>.
- [6] B. Braunn, M. Labalme, G. B. and C. Ray, et al., Nuclear reaction measurements of 95 MeV/u ^{12}C interactions on PMMA for hadrontherapy,
185 Nuclear Instruments and Methods in Physics Research Section B: Beam Interactions with Materials and Atoms 269 (22) (2011) 2676 – 2684. doi:<https://doi.org/10.1016/j.nimb.2011.08.010>.
- [7] J. Dudouet, D. Juliani, M. Labalme, et al., Comparison of two analysis methods for nuclear reaction measurements of $^{12}\text{C} + ^{12}\text{C}$ interactions at
190 95mev/u for hadron therapy, Nuclear Instruments and Methods in Physics

Research Section A: Accelerators, Spectrometers, Detectors and Associated Equipment 715 (2013) 98 – 104. doi:<https://doi.org/10.1016/j.nima.2013.03.038>.

- 195 [8] R. Pleskac, Z. Abou-Haidar, C. Agodi, et al., The first experiment at gsi, Nuclear Instruments and Methods in Physics Research Section A: Accelerators, Spectrometers, Detectors and Associated Equipment 678 (2012) 130 – 138. doi:<https://doi.org/10.1016/j.nima.2012.02.020>.
- [9] M. D. Napoli, C. Agodi, G. Battistoni, et al., Carbon fragmentation measurements and validation of the geant4 nuclear reaction models for hadrontherapy, Physics in Medicine and Biology 57 (22) (2012) 7651–7671. doi:[10.1088/0031-9155/57/22/7651](https://doi.org/10.1088/0031-9155/57/22/7651).
- 200 [10] T. Ogawa, T. Sato, S. e. a. Hashimoto, Energy-dependent fragmentation cross sections of relativistic ^{12}C , Phys. Rev. C 92 (2015) 024614. doi:[10.1103/PhysRevC.92.024614](https://doi.org/10.1103/PhysRevC.92.024614).
- 205 [11] H. Ge, F. Ma, X. Zhang, et al., The production of residual nuclides in pb irradiated by 400mev/u carbon ions, Nuclear Instruments and Methods in Physics Research Section B: Beam Interactions with Materials and Atoms 337 (2014) 34–38. doi:<https://doi.org/10.1016/j.nimb.2014.07.024>.
- [12] L. Chen, F. Ma, X. Zhang, et al., Spallation yield of neutrons produced in thick lead target bombarded with 250mev protons, Nuclear Instruments and Methods in Physics Research Section B: Beam Interactions with Materials and Atoms 342 (2015) 87–90. doi:<https://doi.org/10.1016/j.nimb.2014.09.020>.
- 210 [13] X. Zhang, Y. Zhang, F. Ma, et al., Neutron production for 250 mev protons bombarding on thick grain-made tungsten target, Eur. Phys. J. A 51 (2015) 106. doi:<https://doi.org/10.1140/epja/i2015-15106-0>.
- 215 [14] Y. Q. Ju, X. Y. Zhang, F. Ma, et al., The production of residual radionuclides by a 250 MeV proton beam, Journal of Physics G: Nuclear and

Particle Physics 42 (12) (2015) 125102. doi:10.1088/0954-3899/42/12/
125102.

220

- [15] Z. Sun and W.-L. Zhan and Z.-Y. Guo and et al., Ribll, the radioactive ion beam line in lanzhou, Nuclear Instruments and Methods in Physics Research Section A: Accelerators, Spectrometers, Detectors and Associated Equipment 503 (3) (2003) 496 – 503. doi:[https://doi.org/10.1016/S0168-9002\(03\)01005-2](https://doi.org/10.1016/S0168-9002(03)01005-2).

225

- [16] in: J. Ziegler, J. Biersack (Eds.), The Stopping and Ranges of Ions in Matter, Pergamon, 1980, p. iv. doi:<https://doi.org/10.1016/B978-0-08-021607-2.50004-0>.